Electroabsorption Modulator Using Intersubband Transitions in GaN–AlGaN–AlN Step Quantum Wells

Petter Holmström

***Abstract*—We calculate the high-speed modulation properties of an electroabsorption modulator for $\lambda = 1.55$ μm based on Stark shifting an intersubband resonance in GaN–AlGaN–AlN step quantum wells. In a realistic simulation assuming an absorption linewidth $\Gamma = 100$ meV we obtain an RC-limited electrical $f_{3\mathrm{dB}} \sim 60$ GHz at an applied voltage swing $V_{pp} = 2.8$ V. We also show that a small negative effective chirp parameter suitable for standard single-mode fiber is obtained and that the absorption is virtually unsaturable. The waveguide is proposed to be based on the plasma effect in order to simultaneously achieve a strong confinement of the optical mode, a low series resistance, and lattice-matched cladding and core waveguide layers. Extrapolated results reflecting the decisive dependence of the high-speed performance on the intersubband absorption linewidth Γ are also given. At the assumed linewidth the modulation speed versus signal power ratio is on a par with existing lumped interband modulators based on the quantum confined Stark effect.**

***Index Terms*—III-N materials, intersubband transitions, optical modulators, plasma effect, quantum wells, Stark effect.**

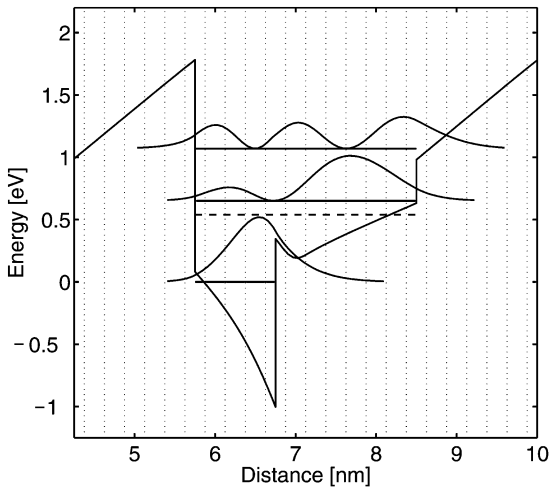

Fig. 1. Potential profile of the second step quantum well including moduli squared of the confined states at zero applied bias voltage. (Dashed line) Fermi level. (Dotted lines) Monolayers.

I. Introduction

OPTICAL modulators are essential components for high-speed optical communication, in that they can avoid the inherent speed limitations of direct modulated interband semiconductor lasers, and in addition extend the transmission distance on optical fibers by providing optical pulses with lower chirp. Current state-of-the-art modulators at the communications wavelength 1.55 μm are based on interband transitions in semiconductor quantum wells using the quantum confined Stark effect (QCSE) [1] and on electro-optic materials such as $LiNbO_3$ in a Mach–Zehnder configuration [2]. However, the former type of modulator has drawbacks concerning the rather low saturation intensity, limiting the launched power into the fiber, and concerning the difficulty of achieving a negative effective chirp parameter, which significantly reduces the dispersion-limited transmission distance on a standard single-mode optical fiber. The electro-optic Mach–Zehnder modulator does not suffer from these drawbacks but requires a rather high modulation voltage swing, which is increasingly difficult to achieve at high speeds. Promising high-speed results have also recently been demonstrated in polymeric modulators [3]. However, the lifetime of the device is still a concern for these modulators.

With the recent demonstrations of intersubband (IS) resonances in InGaAs–AlAsSb [4], GaN–Al(Ga)N [5]–[8], and ZnSe–BeTe [9] quantum wells (QWs) at $\lambda = 1.55$ μm, it is compelling to consider these as a basis for optical modulation. We have previously performed rather extensive theoretical studies of the properties of high-speed modulators based on IS resonances in conventional III–V materials such as InAlAs at $\lambda \sim$ 6–7 μm [10], [11] and GaAs–AlGaAs at $\lambda \sim 9$ μm [12]. And more recently a modulator for 1.55 μm using InGaAs–AlAsSb was also simulated [13], exhibiting promising performance. In general, modulators based on IS transitions in QWs were found to have several potential advantages [11], [14]: a strong material absorption, insensitivity to saturation, tightly confining waveguides can be used (at least at mid-IR and longer wavelengths), and that the applied voltage swing can be symmetric around zero bias. Our previous simulated IS-based modulator for 1.55 μm [13] employed a conventional slab waveguide. But in nitrides the advantage of a tightly confining waveguide may remain also at 1.55 μm, if the plasma effect can be employed to generate a large index contrast and thus provide a strong optical mode confinement also at this wavelength as indeed proposed in this paper. In addition, for long-haul optical communication at 1.55 μm, in this paper we point out that the chirp properties can be very favorable for transmission on a standard single-mode fiber (SSMF), when

Manuscript received April 11, 2006. This work was supported in part by the Japanese Society for the Promotion of Science.

The author is with the KISHINO Laboratory, Department of Electrical and Electronics Engineering, Sophia University, Tokyo 102-8554, Japan, and also with the Department of Microelectronics and Applied Physics, Royal Institute of Technology (KTH), SE-164 40 Kista, Sweden (e-mail: petterh@imit.kth.se).

Digital Object Identifier 10.1109/JQE.2006.877297

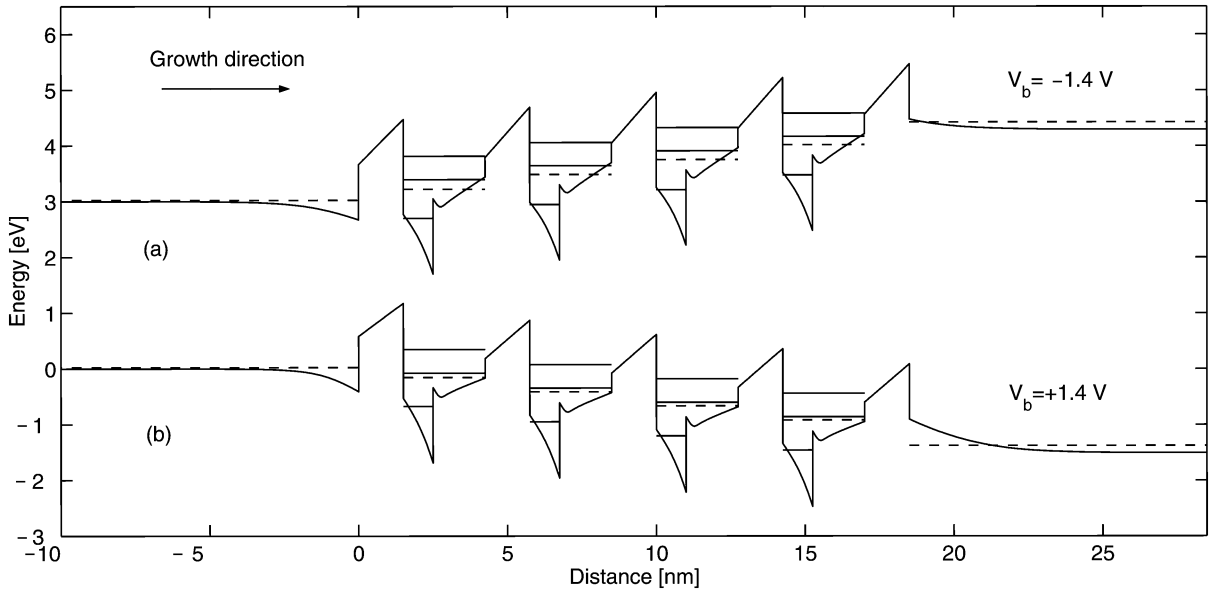

Fig. 2. Potential profile of the modulator structure including the energy levels of the confined states in the step quantum wells. (Dashed lines) Fermi levels. In (a) and (b) the applied bias voltages are $V_b = -1.4$ V and $V_b = 1.4$ V, and the modulator is opaque and transmitting respectively at $\lambda = 1.55$ μm.

using the IS resonance for electroabsorption (EA) modulation. However, the RC-limited modulation speed depends decisively on the IS absorption linewidth Γ that can be achieved, since the modulator capacitance $C \sim \Gamma^3$, whether the EA is based on the Stark effect [11] or quantum interference [12]. Thus a small IS absorption linewidth is required to exploit the above-mentioned advantages and hence be able to realize a fast, low-voltage, and virtually unbleachable modulator with a chirp parameter suitably negative for SSMF.

The purpose of this paper is to find an efficient optical modulator design based on an IS resonance and to compare the predicted performance to existing interband QCSE optical modulators. Stark shifting of the ground state to the first excited state IS transition in an asymmetric step QW is known to be an efficient way to achieve EA. We choose here to simulate a wurtzite GaN–AlGaN–AlN step QW structure (Fig. 1) as grown on, e.g., sapphire. Since GaN is quite new as an IS material with a large spread in demonstrated linewidths Γ, we also provide some simple extrapolations of the simulation results obtained for $\Gamma = 100$ meV.

II. Modulator Structure

A. Multiquantum Well Structure

We evaluate an IS modulator based on Stark shifting the IS resonance, i.e., the IS transition energy is shifted by applying an electric field. An efficient Stark shift requires the QWs to be asymmetrical in order to obtain a nonvanishing dipole moment $e(z_{22} - z_{11})$, between the ground and first excited QW states. Here e is the elementary charge while $z_{ii} = \langle \phi_i | z | \phi_i \rangle$, where ϕ_i, $i = 1, 2$, are the bound QW electron states. In conventional III–V semiconductors, step QWs [11], [15] have been used to obtain an efficient Stark shift, which is then close to linear to the applied electric field. In wurtzite nitride heterostructures there are very strong built-in fields, which does give an asymmetry also to single-layer QWs (e.g., see [16]), but this is not enough for efficient modulation at 1.55 μm, due to the very thin QWs required. Thus we assess here a step QW structure. However, the built-in fields imply that there is a significant difference in the potential profile of a step QW depending on if the deep QW layer or the step layer of the QW is grown first, i.e., they are not only mirror images. We find by simulation that an IS resonance at 1.55 μm should be possible in both cases and moreover that two important properties for electroabsorption, *viz.*, the oscillator strength f_{12} and the dipole moment $e(z_{22} - z_{11})$ that can be achieved are comparable irrespective of the growth order. Though if the AlGaN step layer is grown first (assuming Ga face growth, which is usually desired due to higher material quality) a significantly lower Al concentration is required in this layer. We choose here to evaluate a step QW structure with the deep layer grown prior to the step layer (see Fig. 1). Further we assume that the barriers are pure AlN. The barriers should be thick enough to prevent leakage of carriers when the MQW structure is biased. Then using AlN rather than AlGaN the barriers can be thinner, which reduces the applied voltage that is needed to achieve the Stark shift. It may also be easier to grow by MBE an MQW structure employing just one AlGaN composition (that of the QW step layer) since the need to change the temperature of the Al and/or Ga effusion cells is relaxed. However, MBE systems employing migration-enhanced epitaxy (MEE) could achieve this by appropriate shutter sequences.

In order to obtain a strong IS absorption, the MQW structure must be heavily n-type doped. The IS absorption strength is proportional to the carrier density in the QWs. An interesting question, which however is not considered in any detail here, is the best placement of the dopants. Generally, modulation doped structures with doping in the barriers yield smaller IS absorption linewidths. This has been observed also in GaN–AlGaN single QWs [5]. But in order to effectively reduce broadening by barrier doping, barriers need to be relatively thick. In this paper a δ-doping layer in the well is assumed. Placing the dopants in the QW also allows a higher dopant concentration, however, given the importance of the absorption linewidth for the performance (Section IV-F) it may still prove advantageous to use barrier

TABLE I
DESCRIPTION OF THE LAYERS IN THE SIMULATED DEVICE WITH N-TYPE DOPING DENSITIES. THE LAYERS BETWEEN THE DASHED LINES CONSTITUTE THE ACTIVE LAYER AND ARE TREATED AS AN EFFECTIVE MEDIUM [11] WHEN SOLVING FOR THE OPTICAL MODE

Material	Thickness	Doping
Top contact	-	-
GaN	≈1000 nm	1×10^{20} cm^{-3}
GaN	400	5×10^{18}
$Al_xGa_{1-x}N$, graded	10	5×10^{18}
$Al_{0.52}Ga_{0.48}N$	10	3×10^{19}
AlN	1.5	-
GaN	1.0	-
$Al_{0.85}Ga_{0.15}N$	1.75	7×10^{13} cm^{-2} ×4
AlN	1.5	-
$Al_{0.52}Ga_{0.48}N$	10	5×10^{18} cm^{-3}
$Al_xGa_{1-x}N$, graded	10	5×10^{18}
GaN	400	5×10^{18}
GaN	≈1000	1×10^{20}

doping. The sheet doping concentration is $n_D = 7\times10^{13}$ cm^{-2}. The position of the assumed δ-doping layer is clearly visible in Figs. 1 and 2 as a dip in the potential profile.

On both sides of the MQW structure are AlGaN layers where electrons accumulate or are depleted depending on the applied bias. Hence, as in our previous paper on a mid-IR modulator [11], we call these layers accumulation-depletion layers (ADLs). Though it may be noted that due to the strong built-in fields in the present structure there is always, under the chosen voltage swing, accumulation in one of the layers and depletion in the other as is evident in Fig. 2. As described in the previous paper [11] the ADL composition can be determined to minimize the band bending as seen over the whole MQW, and hence minimize undue spread in the IS transition energies amongst the four step QWs. This problem is seemingly a bit more complex in a nitride-based structure, since the Al-content affects not only the conduction band edge energy but also at the same time the built-in field. However, by simulating self-consistently the whole MQW structure and the surrounding ADLs, it is quite straightforward to, by trying a range of AlGaN compositions, determine which ADL Al-content gives a flat band as seen over the whole MQW, i.e., similar electric field and IS transitions energies in all step QWs. In the present structure this procedure gives the ADL Al mole fraction $x = 0.52$. In order to reduce the depletion layer thickness of the topmost ADL, which as mentioned is always in depletion, a higher doping level, $n_D = 3\times10^{19}$ cm^{-3}, was assumed in that ADL than otherwise in the waveguide core. The complete layer sequence of the simulated structure is shown in Table I.

B. Waveguide and Contacting

A tight confinement of the optical mode is essential in a high-speed modulator, since the required modulator length is inversely proportional to the width of the optical mode. In other words the RC-limited speed can be increased in direct relation to the mode confinement. At least this is true until the thus increased intensity of the optical field leads to absorption saturation in the active layer. But as discussed in Section IV-E IS based material is not prone to saturation, especially not using nitrides. Thus absorption saturation should not be an issue in this modulator.

A strong confinement requires a strong refractive index contrast between the core and cladding layers. That would suggest using AlN, $n = 2.05$, as cladding. However, the cladding must also have a good conductivity in order that the applied voltage is indeed applied over the MQW, and in order to not compromise the modulation speed by a high series resistance. Unfortunately AlN is known to be all but impossible to dope, although in recent breakthroughs an electron density up to 7×10^{17} cm^{-3} was achieved with a low mobility of 11 cm^2/Vs in a highly compensated material [17]. More adequate electron densities and mobilities have been achieved in AlGaN with a 20% Al content [18], but then of course the refractive index contrast compared to the GaN waveguide core is accordingly smaller.

Using the plasma effect (PE) the refractive index can be strongly reduced in a heavily doped material, when the plasma frequency, ω_p [(8)], approaches the frequency of the light, e.g., [19]. Waveguides based on the PE, or at least enhanced by it, or on surface plasmons (SPs) has been used extensively in IS-based devices, notably quantum cascade lasers, for mid-IR and longer wavelengths. Tightly confining waveguides based on the PE at mid-IR wavelengths were proposed and compared to SPs [19]. Efficient waveguides based on the PE at wavelengths as short as $\lambda = 1.55$ μm have not to our knowledge been used or proposed, though weakly confining structures $(\Delta n \sim 0.01)$ in conventional III–V materials were evaluated in the 1970s [20]. However, the reported high electron densities in GaN of up to 1×10^{20} cm^{-3} [21] with low compensation indicates that the PE can yield a substantial refractive index contrast without prohibitive absorption. Another important requirement is a large enough energetic separation of the Γ-valley containing the carriers to the satellite valleys. In GaN the $L-\Gamma$-valley separation is about 2 eV, which should preclude intervalley scattering and also indicates that electron densities $n \sim 5\times10^{20}$ cm^{-3} may be feasible to further reduce the refractive index. Though, at least using MOCVD, the amphoteric nature of Si as a dopant in GaN becomes more apparent at such concentrations, resulting in highly compensated material [21]. Thus, we propose to use a waveguide based on the PE in GaN, with GaN cladding and core layers as described in Table I. The carrier density of $n = 1\times10^{20}$ cm^{-3} at the wavelength $\lambda = 1.55$ μm corresponds to a cladding complex refractive index of $n + ik = 2.11 + i0.011$ [using (8)].

Using the PE rather than a compositional heterostructure has the advantage that it can achieve the combination of the following:

1) a high refractive index contrast ($\gtrsim 10\%$);
2) excellent conductivity of the cladding layer;
3) lattice matching of cladding and core layers.

On the downside is a higher waveguide absorption for a tightly confining waveguide, but it appears acceptable in a short modulator. In comparison a SP-based waveguide at this short wavelength would entail several times higher waveguide absorption.

The required modulator length for 10-dB extinction ratio is only $L = 13$ μm in the considered structure with the assumed IS absorption linewidth $\Gamma = 100$ meV. To avoid stray light

TABLE II
PARAMETER VALUES [23]–[27] EMPLOYED IN THE SIMULATION

Parameters	GaN	AlN
ΔE_c [eV]	-	1.7
E_g [eV]	3.4	6.2
m_e	0.22	0.30
ε_s (|| c)	10.4	8.5
n	2.3	2.05
P_{sp} [C/m^2]	-0.034	-0.090
e_{33} [C/m^2]	0.67	1.50
e_{31} [C/m^2]	-0.34	-0.53
C_{33} [GPa]	354	377
C_{31} [GPa]	68	94
a [Å]	3.189	3.112
c [Å]	5.185	4.982

being transmitted outside such a short modulator passive waveguide sections can be added. The modulator structure would then be etched down outside of the active length and, for example, an AlN–GaN–AlN waveguide would be regrown for the passive sections. Such passive waveguides could also further facilitate coupling by allowing lateral tapering of the waveguide and somewhat increased waveguide thickness in the passive sections. Coupling losses to such passive sections can be low as noted in Section IV-A. However, apart from this, only the active modulator part is considered in this paper.

The small size of the present modulator necessitates a low resistivity contact on top of the mesa. Ohmic contacts with a low resistivity of $9\times10^{-8}\,\Omega\cdot\text{cm}^2$ have been demonstrated using Ti–Al on n–GaN [22]. This corresponds to a clearly acceptable resistance of just under $1\ \Omega$ for the top contact.

III. MODEL

A prominent feature in wurtzite nitrides grown along the [0001] direction (the c axis) is the strong material polarization. Spontaneous and strain-induced, i.e., piezoelectric, polarizations result in very strong built-in fields in heterostructures. The spontaneous polarization P_{sp} of AlGaN is interpolated linearly using data in Table II. In a structure with biaxial strain the piezoelectric polarization in the growth direction is readily obtained as

$$P_{pz} = e_{33}\epsilon_c + 2e_{31}\epsilon_a \tag{1}$$

where $\epsilon_a = (a_0 - a)/a$ and $\epsilon_c = -2C_{13}/C_{33}\epsilon_a$ are the strains in the plane and the growth direction, respectively. Here a_0 is the lateral lattice-parameter of the GaN buffer, while a is the native lattice-parameter of each layer material. The Al-containing active layer (i.e., the MQW) and the ADLs are thus assumed to be grown lattice-matched to the underlying GaN waveguide core layer. Experimentally GaN–AlGaN heterostructures support relatively thick strained layers [28], [29], compared to the experience from conventional III–V semiconductors, e.g., in [28] a 600-nm $Al_{0.104}Ga_{0.896}N$ layer was grown coherently on GaN.

The assumed conduction band offset ($\Delta E_c = 1.7$ eV) is a conservative estimate for pseudomorphic GaN–AlN. In determining a suitable composition for the QW step layer material and the ADLs we use an AlGaN conduction band bowing parameter of 0.7 eV [30], i.e.,

$$\Delta E_c(x) = 1.7x - 0.7x(1-x)\ \text{eV}. \tag{2}$$

We use the envelope function approximation [31] to obtain the confined electron states in the step QW:s. Parabolic subbands with parallel masses $m_{e1} = 0.31$ and $m_{e2} = 0.35$ where assumed in calculating the subband populations in the step QWs. The potential profile and the electron densities of the whole active region, including the MQW structure as well as the adjoining ADL:s are obtained self-consistently using the Poisson's equation as illustrated by Fig. 2. This allows to accurately determine the electric field over the step QWs as a result of the applied voltage. Room-temperature ($T = 300$ K) was assumed in calculating the Fermi levels.

We model the wavelength dependent permittivity in each QW as previously in [11]

$$\epsilon_z = \epsilon_\infty - f_{12}\frac{\epsilon_\infty\omega_{p,z}^2}{\omega^2 - \omega_{12}^2 + i\gamma\omega} \tag{3}$$

$$\epsilon_x = \epsilon_\infty - \frac{\epsilon_\infty\omega_{p,x}^2}{\omega^2 + \frac{i\omega}{\tau_w}} \tag{4}$$

where f_{12} is the oscillator strength given by (6) in [32]. In the plasma frequency

$$\omega_{p,z}^2 = \frac{(n_1 - n_2)e^2}{\epsilon_\infty\epsilon_0 m_0 L_w} \tag{5}$$

we may consider quenching due to band filling, i.e., n_1 and n_2 are the sheet densities in the ground and first excited states, respectively. Further m_0 is the free electron mass and $L_w = 2.75$ nm is the QW width. The background dielectric constant $\epsilon_\infty = n_w^2$, where $n_w = 2.2$ is a refractive index relevant for the step QW material. The transition energy $\hbar\omega_{12} = E_2 - E_1$ and $\hbar\gamma = \Gamma = 100$ meV is a phenomenological IS resonance linewidth parameter. In the Drude expression (4) for ϵ_x, the plasma frequency is given by

$$\omega_{p,x}^2 = \frac{n_1 e^2}{\epsilon_\infty\epsilon_0 m_{e1} m_0 L_w} \tag{6}$$

and $\tau_w = 20$ fs is the electron dephasing time. The precise value of this dephasing time is not important here as it has a negligible influence on the final results.

The IS absorption as determined from (3) corresponds to a Lorentzian lineshape, which is used for simplicity. Experimentally IS resonances are subjected to a combination of finite-lifetime broadening and inhomogeneous broadening resulting in Lorentzian and Gaussian lineshapes, respectively. However, the absorption spectra of coupled QWs containing two IS transitions was recently well fitted to a sum of two Lorentzians [16]. The linewidth $\Gamma = 100$ meV, appears possible in a high-quality step QW material. However, given the decisive importance of the absorption linewidth on notably the high-speed properties, extrapolations of the simulation result depending on the linewidth Γ are given in Section IV-F.

The optical mode and modal absorption was obtained by the transfer matrix method in the same manner as in our previous paper [11]. Since the MQW periodicity is much smaller than the wavelength, an effective medium approximation was used for the complex permittivity of the MQW structure [11].

As discussed in Section II-B we assume a waveguide based on the PE in heavily doped GaN. We are then faced with assessing the electron scattering time in order to estimate the free-carrier absorption (FCA) in the doped layers. In our previous papers (e.g., [19]) a quantum mechanical calculation was employed to obtain such scattering times relating to LO-phonons and ionized impurities in conventional III–V materials. However, since the material quality of the III-nitrides is generally significantly lower, with, for example, a high density of dislocations, it is appealing to obtain the scattering time from available experimental data for the electron mobility, hence accounting for all scattering processes as well as for any compensation in the doping. In the relaxation time approximation applicable for elastic or nearly elastic scattering events, such as impurity scattering which should dominate in a heavily doped material, the scattering time is given by

$$\tau = \mu m_e \frac{\left(1 + \frac{2E_F}{E_g}\right)}{e} \tag{7}$$

where E_F is the Fermi energy and the term $2E_F/E_g$ accounts for the nonparabolicity. The mobility of n-doped GaN is $\mu = 100\,\mathrm{cm}^2/\mathrm{Vs}$ at $n = 1\times10^{20}\,\mathrm{cm}^{-3}$ [21], implying the scattering time $\tau = 15$ fs using (7). The PE is modeled by the classical Drude model[1]

$$(n+ik)^2 = \epsilon = \epsilon_\infty \left[1 - \frac{\omega_p^2}{\omega^2}\left(1 - \frac{i}{\omega\tau}\right)\right] \tag{8}$$

where ω_p is an effective plasma frequency [19], accounting for the conduction band nonparabolicity of the heavily doped bulk GaN material by assuming hyperbolic bands. Using a single scattering time τ as is done here, hence neglecting its dependence on the photon energy in the FCA process [33], gives the classical λ^2-dependence of the FCA, and is likely to overestimate the FCA. This is confirmed by a measured FCA of 300 cm^{-1} in MOCVD GaN at the photon energy $\hbar\omega = 0.8$ eV and electron concentration 5×10^{19} cm^{-3} [34], whereas the present model gives 1000 cm^{-1} for those parameters, assuming $\mu = 100\ \mathrm{cm}^2/\mathrm{Vs}$.

IV. Results

A. Absorption Modulation

The absorption modulation around $\lambda = 1.55\ \mu$m is achieved by Stark shifting the ground state to first excited state $(1 \rightarrow 2)$ IS resonance (Fig. 3). Since an IS resonance is peak shaped, in contrast to the step like absorption spectrum of QW interband transitions, there is in principle a choice when employing the Stark effect as to using the high- or low-energy flank of the IS resonance for absorption modulation. However, the following several factors support using the high-energy flank as in this paper.

1) It requires a lower IS transition energy, which is more easily realized.
2) It achieves a negative effective chirp parameter as discussed in Section IV-B.
3) The oscillator strength is in general increased when the IS transition is Stark shifted to higher energy, thus yielding a stronger absorption modulation on the high-energy flank.

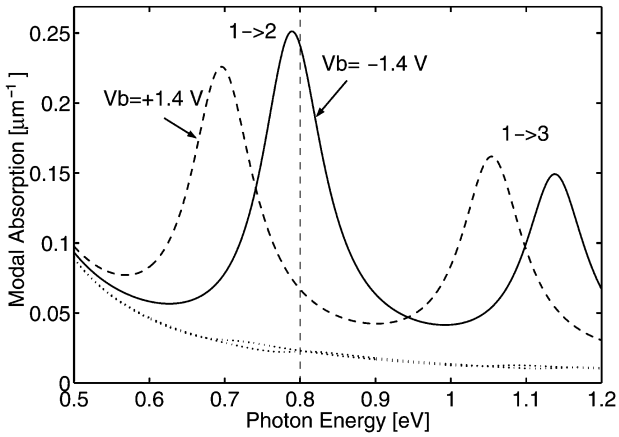

Fig. 3. Modal absorption spectrum in the modulator at the applied bias voltages $V_b = -1.4$ V (solid) and $V_b = 1.4$ V (dashed). The dotted lines show the waveguide absorption, α_w, at these respective bias voltages. The vertical dashed line indicates the photon energy, $\hbar\omega = 0.8$ eV ($\lambda = 1.55\ \mu$m), of the input optical field.

Under the application of the voltage swing the IS resonance energy is shifted from 698 meV at $V_b = 1.4$ V to 792 meV at $V_b = -1.4$ V. The IS resonance energy includes a sizeable depolarization blue shift (~ 90 meV), with respect to the single-particle IS transition energy $\hbar\omega_{12}$, due to the high electron concentration in the step QWs. A simple account (slab model) [35] of the depolarization is inherent in the model. Under the voltage swing the oscillator strength f_{12} at the same time increases from 1.99 ($V_b = 1.4$ V) to 2.23 ($V_b = -1.4$ V) thus enhancing the absorption modulation. The carrier densities in the step QWs are $n_1 = 6.9\times10^{13}\ \mathrm{cm}^{-2}$ and $n_2 < 1\times10^{11}\ \mathrm{cm}^{-2}$ respectively, irrespective of the bias. The polarization dependence of conduction band IS transitions implies that modulation is achieved for TM polarized light. Thus the modulator requires a highly linearly polarized optical input. This can be achieved by placing the modulator, as is often done, close to the laser. The waveguide absorption resulting from FCA in the heavily doped cladding layers is also indicated in Fig. 3. As mentioned above in Section III this is likely overestimated. Hence it appears that the PE in GaN can be used without a prohibitive FCA in the present modulator.

The active length of the modulator is determined by a required 10-dB extinction ratio, i.e., that $\Delta\alpha_m L = 2.3$. From Fig. 3 we have $\Delta\alpha_m = 0.17\ \mu\mathrm{m}^{-1}$ for the applied voltage swing $V_b = \pm1.4$ V, and thus an active length as short as $L = 13\ \mu$m. For this active length the transmission loss 3.8 dB at $V_b = 1.4$ V, due to residual IS absorption and FCA in the cladding layers, is

[1]In keeping with (3) and (4) we assume here a negative sign in the time evolution of the optical field, i.e., $\exp(-i\omega t)$. Hence, the difference in the sign of the imaginary parts of the dielectric constant ϵ and the complex refractive index $(n + ik)$ in (8) compared to our previous paper [19].

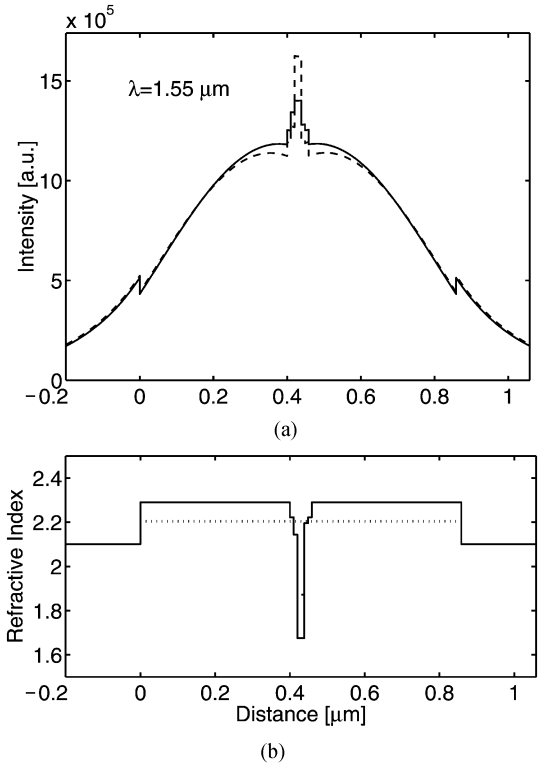

Fig. 4. (a) Mode intensity profiles and (b) profile of the refractive index in the direction perpendicular to the layers. The dotted line in the lower panel is the mode index. The results are for $V_b = -1.4$ V (solid) and $V_b = 1.4$ V (dashed).

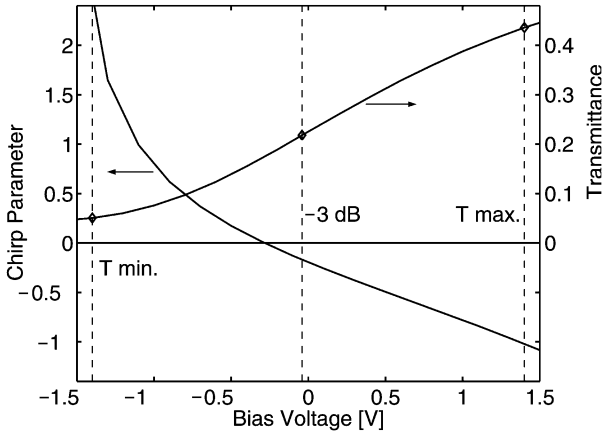

Fig. 5. Modulator chirp parameter α and transmittance T versus the applied voltage. Dashed lines indicate the applied voltage swing with minimum and maximum transmittance T at $V_b = -1.4, +1.4$ V respectively, and where T has dropped by 3 dB.

also readily obtained from Fig. 3. As discussed in Section II-B passive waveguide sections would probably be required to avoid transmission of stray light outside the short modulator. The additional coupling losses from such passive sections can be made very small, e.g., less than 1 dB in conventional III–V materials [36].

The transverse intensity profile of the optical mode is shown in Fig. 4. The mode overlap with the active layer is quite modest, e.g., $\Gamma_{\mathrm{MQW}} = 5.2\%$ in the opaque state $(V_b = -1.4$ V). The lower refractive index in the cladding layers are due to the PE in heavily doped GaN $\left(n_D = 1 \times 10^{20}\ \mathrm{cm}^{-3}\right)$ as discussed in Section II-B. If higher electron concentrations can be achieved this refractive index can be reduced considerably. Thus enhancing the mode confinement, though the confinement as judged by the mode width is already quite adequate.

B. Chirp Parameter

In current fiber-optic communication systems employing Er-doped fiber amplifiers the chromatic dispersion usually limits the performance. The dispersion penalty becomes increasingly severe at high bitrates B, as the dispersion-limited transmission length $L_d \sim 1/B^2$. For example at $B = 40$ Gb/s assuming zero chirp pulses on SSMF L_d is only about 4 km. However, this distance depends strongly on the phase modulation that in general accompanies the amplitude modulation in optical modulators [37], [38]. The amount of frequency chirp thus given to emitted optical pulses can be characterized by the modulator chirp parameter α [38]. A small negative chirp α is desirable on SSMF around 1.55 μm. Unfortunately direct modulated semiconductor lasers tend to have a large positive chirp parameter $(\alpha \sim 2)$ which is indeed one of the motivations for using external modulators. However, it is interesting to note that IS-based lasers in general have close to zero chirp as a result of a symmetric IS gain spectrum [39].

The bias voltage dependent chirp parameter of an EA modulator can be obtained as

$$\alpha(V_b) = \frac{dn_m}{dk_m} \tag{9}$$

where n_m and k_m are the real and negative imaginary parts respectively of the modal refractive index. The chirp parameter calculated according to (9) together with the transmittance of the modulator is shown in Fig. 5. The chirp parameter α is negative at high transmittance, while it becomes positive at low transmittance. This is interesting since it has been shown that the chirp parameter at high transmittance is more important, and the average of the chirp during the top 3 dB of transmittance were suggested as an effective chirp parameter [37]. Using that procedure we determine a small negative effective chirp parameter $\alpha_{\mathrm{eff}} = -0.6$, which is close to optimal on SSMF. We note that the negative chirp at high transmittance and hence a negative α_{eff} is a direct consequence of using the high-energy flank of the IS resonance. In contrast interband QCSE modulators, which naturally must use the low-energy side of the band-edge absorption step in that case, tend to have positive chirp at high transmittance and negative at low transmittance, e.g., [40]. Hence employing the interband QCSE there is a tradeoff that lower chirp can be achieved by accepting higher insertion loss, but a negative effective chirp is in general not achieved. Using the IS-based Stark effect such a tradeoff becomes unnecessary in the present modulator as the more negative chirp and the high transmittance is achieved in the same region of the voltage swing, viz., when the IS resonance is tuned away from the photon energy. We note that the modulator structure considered here, based on Stark shift in a step QW, appears to have a better chirp performance than the modulator structure that we evaluated in [13]. It is also noteworthy that the transmittance curve in Fig. 5 has a desirable S-shape, being steeper in the middle of the voltage swing, thus to some extent suppressing noise in the bias voltage.

C. Electrical Properties

The results obtained thus far are steady-state properties. The modulation speed of this modulator, which does not rely on carrier transport within the MQW structure, is limited by the RC time constant of the driver-modulator circuit.

We can obtain the capacitance as $C = eLw(\Delta n_l - \Delta n_r)/2V_{pp}$, where $w = 1.0$ μm is the modulator (mesa) width and Δn_l (Δn_r) is the change in sheet electron density (depletion counted as negative) in the left (right) ADL under the application of the whole voltage swing $V_{pp} = 2.8$ V. For the present structure we obtain $C = 52$ fF. In order to fully benefit from this low capacitance the parasitic capacitances must of course be brought down well below this level. This does not appear to be completely impracticable. However, the parasitics are not considered further here.

The series resistance of the modulator will be mainly due to the contact resistance of the ohmic top contact and to the two GaN waveguide core layers with the total thickness $d_c = 0.8$ μm, i.e., $R_s \approx \rho_s/wL + d_c/wLen\mu = 1\ \Omega + 4\ \Omega = 5\ \Omega$. Here we assumed a specific contact resistance $\rho_s = 9\times10^{-8}\ \Omega \cdot \mathrm{cm}^2$ [22], and the core layer doping $n = 5 \times 10^{18}$ cm^{-3} and mobility $\mu = 200$ cm^2/Vs [21].

The electrical properties of the driver-modulator circuit can be assessed in a simple lumped circuit model [11]. The electrical $f_{3\mathrm{dB}} = 1/2\pi RC$ for small signals is defined as a 3-dB decrease in the received detector signal. With a standard driver impedance of $R_0 = 50\ \Omega$ and not considering a shunt (termination) resistance, we have $R = R_0 + R_s = 55\ \Omega$ and $f_{3\mathrm{dB}} \approx 60$ GHz. We can consider this as a good estimate also for the large signal modulation speed [11]. As mentioned in [11] the symmetric voltage swing of intersubband modulators, in contrast to interband-based EA modulators, implies that driving with transistors in a balanced configuration is more easily achieved. A balanced transistor amplifier output, in effect doubling the useful voltage swing, relaxes the requirements on the transistor breakdown voltage, thus allowing smaller higher speed transistors.

D. Figure of Merit

It is now interesting to compare the present simulation results to current state-of-the-art *interband*-based EA modulators. The speed-power ratio $f_{3\mathrm{dB}}/P_{ac}$, where the electrical signal power $P_{ac} = V_{pp}^2/8R_0$, is a relevant figure of merit in the context of an RC-limited EA modulator. This can be motivated by that the required voltage swing V_{pp} can be chosen according to the number of QWs employed in the MQW structure, which in turn will affect the modulation speed according to $f_{3\mathrm{dB}} \sim V_{pp}^2$ [11]. Hence the speed-power ratio depends on the design of the QW EA material and the waveguide, and is at least approximately invariant to the choice of number of QWs.

In the present simulation the speed-power ratio $f_{3\mathrm{dB}}/P_{ac} = 3.2$ GHz/mW. In interband QCSE lumped electroabsorption modulators there are a few demonstrations of $f_{3\mathrm{dB}}$ around 50 GHz in the last decade, e.g., Ido *et al.* [36] reported a modulator with $f_{3\mathrm{dB}} \approx 50$ GHz at $V_{pp} = 2.5$ V yielding $f_{3\mathrm{dB}}/P_{ac} = 3.2$ GHz/mW, same as in the here simulated modulator. Their device had a higher extinction ratio of 15 dB, requiring longer modulator length, thus increasing capacitance. However, considering also that a 50-Ω termination resistor was used in [36] on their 10-Ω series resistance device, these two effects on the RC-limitation nearly cancel. Figures of merit for optical modulators should be used with some caution since there are generally tradeoffs to be made, e.g., the speed can in general be increased at the expense of insertion loss. But the above comparison indicates that the speed-power ratio figure of merit of the simulated IS-based modulator is approximately on a par with high-performance lumped interband QCSE modulators. We should emphasize that this result was obtained at the assumed IS absorption linewidth $\Gamma = 100$ meV. As discussed in Section IV-F, the achievable speed of the simulated IS modulator depends decisively on the IS linewidth. It can also be noted that somewhat higher speed-power ratios have been demonstrated in interband QCSE modulators in a traveling wave configuration, e.g., [1]. But such comparisons would be beyond the scope of this paper, which considers a lumped RC-limited device. In a previous simulation [13] of an IS-based electroabsorption modulator for $\lambda = 1.55$ μm using InGaAs–AlAsSb coupled QWs we obtained $f_{3\mathrm{dB}} \approx 90$ GHz at $V_{pp} = 2.0$ V (and assuming a linewidth $\Gamma = 60$ meV), i.e., $f_{3\mathrm{dB}}/P_{ac} = 9$ GHz/mW.

E. Absorption Saturation and Thermal Properties

One important advantage that has been predicted for IS-based modulators [11] compared to the interband-based QCSE type is the high optical powers tolerable without absorption saturation. The high absorption saturation power results from the rapid IS relaxation, allowing electrons excited from the first subband to the second to effectively relax and be "recycled" within the same QW. In contrast in interband-based QCSE modulators with about four orders of magnitude longer relaxation times (over the bandgap in that case) electron and holes generated in the absorption process need to be efficiently swept out of the MQW region to avoid absorption saturation. Especially for the holes that is a problem leading to absorption saturation due to hole pile-up.

The absorption saturation intensity of a two level system is given by (right-hand-side equality)

$$\frac{\Gamma_{\mathrm{MQW}} P_s}{d_{\mathrm{MQW}} w} = I_s = \frac{\hbar\omega}{2\sigma T_1} \tag{10}$$

where σ is the absorption cross section-section and T_1 is the IS relaxation time. The left-hand-side equality of (10) relates I_s to the saturation power P_s, where d_{MQW} is the thickness of the MQW. If we then consider that the part of the modal absorption that is due to IS transitions (i.e., disregarding the waveguide absorption, which does not lead to IS absorption saturation) is $\alpha_{m,IS} = \Gamma_{\mathrm{MQW}}(n_s/d_{\mathrm{MQW}})\sigma$, where $n_s = 4n_1$ is the total sheet electron concentration in the four step QW:s, we can rearrange to get

$$P_s = \frac{w n_s \hbar\omega}{2\alpha_{m,IS} T_1}. \tag{11}$$

From Fig. 3 we have the maximum $\alpha_{m,IS} = 0.22$ μm^{-1}. The IS scattering time in GaN–AlGaN QW:s at telecommunications wavelengths was recently measured at $T_1 = 140$ fs [41]. This implies that the optical saturation power of the modulator is as huge as $P_s = 6$ W(!). This is about three orders of magnitude

higher than the saturation power of interband QCSE modulators, which is typically several milliwatts. The huge saturation power of the modulator analyzed here should however not be too surprising, since it is in accordance with the quite high optical pulse energies required to operate all-optical modulators based on ISTs in GaN–AlN QWs [42]. GaN being a highly polar semiconductor with large electron mass, $m_e = 0.22$, and LO-phonon energies, $\hbar\omega_{\rm LO} \approx 90$ meV, exhibits very fast carrier dynamics. Indeed among the QW materials where IS resonances at 1.55 μm have been demonstrated GaN has the most rapid carrier dynamics, and notably the shortest IS relaxation time.

Obviously it is thermally inconceivable to dissipate a multiwatt power within the small modulator structure. The thermal conductivity of GaN is very good at $\sim$ 1–2 W/cm K. However, in sapphire, the most prevalent substrate for GaN, it is quite poor at 0.23 W/cm K ($\|$ c axis). The small footprint of the active area of the modulator (13×1 μm^2) then results in a thermal impedance of the simulated device of about 5 K/mW. Using instead SiC as a substrate, which is also attractive for growth of wurtzite GaN, however about an order of magnitude more costly, its high thermal conductivity of 3.8 W/cm K yields a device thermal impedance of about 1 K/mW. In recent experimental results the IS absorption even in a low-bandgap and hence high-nonparabolicity material, InAs/AlSb, is remarkably insensitive to temperatures up to 700 K [43]. Accepting say a heating of 100 K above room temperature we expect that optical and electrical powers of about 20 mW (100 mW) can be handled by the modulator when grown on a sapphire (SiC) substrate, without significant degrading of the performance, or of the structure itself, due to heating.

There is also heating due to the input microwave signal. During one cycle of the input signal the switching energy $E_{sw} = CV_{pp}^2 = 0.4$ pJ must be dissipated due to charge and discharge of C. If we as a worst case assume the frequency $f = f_{3\rm dB} = 1/2\pi RC$, we obtain an upper limit for the dissipated electrical power $P_{sw} = V_{pp}^2/2\pi R = 23$ mW, which is actually independent of the capacitance. However, out of this only the fraction $R_s/R \approx 10\%$ is dissipated within the modulator and should have a negligible effect.

Thus the input power limitation in the present device is due to heating not, as for interband QCSE, absorption saturation. A power limitation of 20 mW as obtained for a sapphire substrate is significantly more than typically achieved in interband QCSE, and more than enough for fiber optical communication requirements.

F. Significance of the Linewidth

A small IS absorption linewidth is of vital importance to achieve high-speed modulation. As we have previously obtained [11] for IS-based Stark effect modulators the achievable device capacitance depends decisively on the absorption linewidth Γ. When the optical mode confinement is largely independent of the active layer, as is well satisfied in the present structure, we have [11]

$$C \sim \frac{\Gamma^3}{V_{pp}^2}. \tag{12}$$

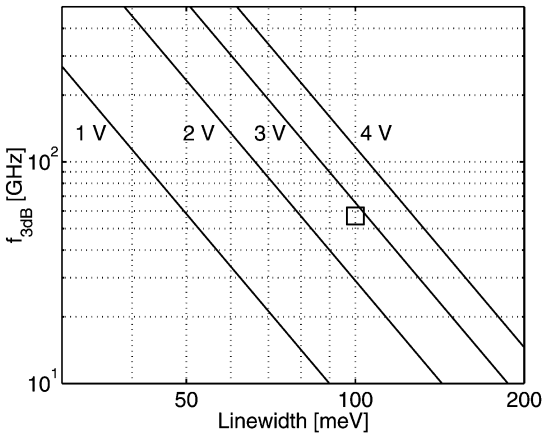

Fig. 6. RC-limited modulation frequency $f_{3\rm dB}$ plotted versus achieved absorption linewidth Γ for a few applied voltage swings V_{pp}. The square indicates the present simulation result.

We note that (12) results by considering that the number of step QWs to use in the structure (under the constraint of an appropriate size Stark shift) is $n_{\rm QW} \sim V_{pp}/\Gamma$. Of course (12) should not be taken to mean that the capacitance is dependent on the linewidth or voltage swing in a given device. Hence employing this simple relation, the RC-limited modulation speed can be extrapolated from the present simulation result as illustrated by Fig. 6, in the case of linewidths other than $\Gamma = 100$ meV, or when the number of step QWs is different from 4. Moving vertically up in this diagram means increasing the number of step QWs in the structure, hence increasing the required voltage swing V_{pp} at a given linewidth Γ. For example we see that, according to this simulation, achieving $f_{3\rm dB} = 40$ GHz at $V_{pp} = 1$ V would require an absorption linewidth Γ of just under 60 meV.

It follows directly from (12) that the speed-power ratio figure of merit depends as decisively on the IS resonance linewidth, i.e.,

$$\frac{f_{3\rm dB}}{P_{ac}} \sim \Gamma^{-3}. \tag{13}$$

As noted above in Section IV-D the speed-power ratio is independent of the voltage swing V_{pp}. In (13) we neglected the Γ dependence of the series resistance R_s, since R_s has a marginal influence ($< 10\%$) on $f_{3\rm dB}$.

Experimentally, the smallest observed IS linewidth in GaN–AlN QWs at, or at least overlapping with, $\lambda = 1.55$ μm is $\Gamma = 60$ meV reported very recently [8]. At the small well width required for IS resonances at 1.55 μm the linewidth is dominated by interface roughness scattering and inhomogeneous broadening due to well-width fluctuations. Thus there is still a significant potential for improvement of IS resonance linewidths in GaN-based QWs, if a suitable lattice-matched substrate material becomes available, and by further improving growth conditions. It can be expected however that the IS resonance linewidth is somewhat larger in step QWs, since they are inherently more sensitive to fluctuations in the transverse electric field. The high doping density required for strong IS absorption also generally increase broadening, and thus the

dopant density and position are also important parameters for the linewidth. Optimizing these is the subject of future research.

V. Conclusion

We have simulated an electroabsorption modulator for $\lambda = 1.55\ \mu$m based on Stark shifting an intersubband resonance in GaN–AlGaN–AlN step QWs. The RC-limited speed is $f_{3\mathrm{dB}} \approx 60$ GHz at an applied voltage swing of $V_{pp} = 2.8$ V. We also showed that a small negative effective chirp parameter (near perfect for standard single-mode fiber) results when Stark shifting the IS resonance, and that the modulator is practically unbleachable with a high thermally limited optical input power. The speed-power ratio of 3.2 GHz/mW is approximately on a par with present high-performance lumped interband QCSE modulators at the assumed IS linewidth of $\Gamma = 100$ meV, and increases strongly ($\sim \Gamma^{-3}$) with reduced IS linewidth. The main challenge is thus to achieve a narrow IS linewidth, in the high doping condition required for a strong IS absorption.

Concerning waveguide cladding, to overcome the problem of low electron density and mobility in AlGaN, we proposed to use the plasma effect in heavily doped GaN to achieve cladding layers with high index contrast, low series resistance and lattice matching to the core layer. Further, the whole active region including the MQW and the adjoining layers were simulated self-consistently. This allowed us to show that despite large built-in fields it is possible to achieve near equal applied electric fields over the step QWs, by proper choice of the composition in the adjoining AlGaN layers.

References

[1] R. Lewen, S. Irmscher, U. Westergren, L. Thylen, and U. Eriksson, "Segmented transmission-line electroabsorption modulators," *J. Lightw. Technol.*, vol. 22, no. 1, pp. 172–179, Jan. 2004.

[2] K. Kondo, A. Kondo, K. Aoki, S. Takatsuji, O. Mitomi, M. Imaeda, Y. Kozuka, and M. Minakata, "High-speed and low-driving-voltage x-cut $LiNb0_3$ optical modulator with two step backside slot," *Electron. Lett.*, vol. 38, no. 10, pp. 472–473, 2002.

[3] W. H. Steier, A. Szep, Y.-H. Kuo, P. Rabiei, S.-W. Ahn, M.-C. Oh, H. Zhang, C. Zhang, H. Erlig, B. Tsap, H .R. Fetterman, D. H. Chang, and L. R. Dalton, "High speed polymer electro-optic modulators," in *14th Annu. Meeting of the IEEE Lasers and Electro-Optics Soc.*, 2001, vol. 1, pp. 188–189.

[4] T. Mozume, H. Yoshida, A. Neogi, and M. Kudo, "1.55 μm intersubband absorption in InGaAs–AlAsSb grown by molecular beam epitaxy," *Jpn. J. Appl. Phys.*, vol. 38, no. 2B, pp. 1286–1289, 1999.

[5] C. Gmachl, H. M. Ng, S.-N. G. Chu, and A. Y. Cho, "Intersubband absorption at $\lambda \sim 1.55\ \mu$m in well- and modulation-doped GaN–AlGaN multiple quantum wells with superlattice barriers," *Appl. Phys. Lett.*, vol. 77, no. 23, pp. 3722–3724, 2000.

[6] K. Kishino, A. Kikuchi, H. Kanazawa, and T. Tachibana, "Intersubband absorption at $\lambda \sim 1.2$–$1.6\ \mu$m in GaN–AlN multiple quantum wells grown by RF-plasma molecular beam epitaxy," *Phys. Stat. Sol. (a)*, vol. 192, no. 1, pp. 124–128, 2002.

[7] N. Iizuka, K. Kaneko, and N. Suzuki, "Near-infrared intersubband absorption in GaN–AlN quantum wells grown by molecular beam epitaxy," *Appl. Phys. Lett.*, vol. 81, no. 10, pp. 1803–1805, 2002.

[8] I. Friel, K. Driscoll, E. Kulenica, M. Dutta, R. Paiella, and T. D. Moustakas, "Investigation of the design parameters of AlN–GaN multiple quantum wells grown by molecular beam epitaxy for intersubband absorption," *J. Crystal Growth*, vol. 278, no. 1-4, pp. 387–392, 2005.

[9] R. Akimoto, Y. Kinpara, K. Akita, F. Sasaki, and S. Kobayashi, "Short-wavelength intersubband transitions down to 1.6 μm in ZnSe/BeTe type-II superlattices," *Appl. Phys. Lett.*, vol. 78, no. 5, pp. 580–582, 2001.

[10] P. Holmström, L. Thylén, and U. Ekenberg, "Proposal of an optical modulator based on resonant tunneling and intersubband transitions," *IEEE J. Quantum Electron.*, vol. 37, no. 2, pp. 224–230, Feb. 2001.

[11] P. Holmström, "High-speed mid-IR modulator using Stark shift in step quantum wells," *IEEE J. Quantum Electron.*, vol. 37, no. 10, pp. 1273–1282, Oct. 2001.

[12] P. Jänes, P. Holmström, and U. Ekenberg, "A high-speed intersubband modulator based on quantum interference in double quantum wells," *IEEE J. Quantum Electron.*, vol. 38, no. 2, pp. 178–184, Feb. 2002.

[13] P. Jänes and P. Holmström, "High-speed optical modulator based on intersubband transitions in InGaAs–InAlAs–AlAsSb coupled quantum wells," in *Proc. 15th Int. Conf. Indium Phosphide and Related Materials*, 2003, pp. 308–311.

[14] P. Holmström, High-speed optical modulators based on intersubband transitions. Stockholm, Sweden, Dept. Microelectronics and Inf. Technol., Roy. Inst. Technol. (KTH), 2003, Ph.D. dissertation.

[15] R. P. G. Karunasiri, Y. J. Mii, and K. L. Wang, "Tunable infrared modulator and switch using Stark shift in step quantum wells," *IEEE Electron. Device Lett.*, vol. 11, no. 5, pp. 227–229, May 1990.

[16] C. Gmachl, H. M. Ng, and A. Y. Cho, "Intersubband absorption in degenerately doped GaN–$Al_xGa_{1-x}N$ coupled double quantum wells," *Appl. Phys. Lett.*, vol. 79, no. 11, pp. 1590–1592, 2001.

[17] T. Ive, O. Brandt, H. Kostial, K. J. Friedland, L. Däweritz, and K. H. Ploog, "Controlled n-type doping of AlN:Si films grown on 6H-SiC(0001) by plasma-assisted molecular beam epitaxy," *Appl. Phys. Lett.*, vol. 86, pp. 024106–024106, 2005.

[18] M. Ahoujja, J. L. McFall, Y. K. Yeo, R. L. Hengehold, and J. E. Van Nostrand, "Electrical and optical investigation of MBE grown Si-doped $Al_xGa_{1-x}N$ as a function of Al mole fraction up to 0.5," *Mater. Sci. Eng.*, vol. B91-92, pp. 285–289, 2002.

[19] P. Holmström, "High-confinement waveguides for mid-IR devices," *Physica E*, vol. 7, no. 1–2, pp. 40–43, 2000.

[20] E. Garmire, "Semiconductor components for monolithic applications," in *Integrated Optics*, T. Tamir and E. Garmire, Eds. Berlin, Germany: Springer-Verlag, 1975, vol. 7, Topics in Applied Physics.

[21] J. H. Edgar, Ed., *Properties of Group III Nitrides*. London, U.K.: INSPEC, 1994, vol. 11, EMIS Datareviews Series.

[22] Z. Fan, S. N. Mohammad, W. Kim, Ö. Aktas, and A. E. Botchkarev, "Very low resistance multilayer ohmic contact to n-GaN," *Appl. Phys. Lett.*, vol. 68, no. 12, pp. 1672–1674, 1996.

[23] I. Vurgaftman, J. R. Meyer, and L. R. Ram-Mohan, "Band parameters for III–V compound semiconductors and their alloys," *J. Appl. Phys.*, vol. 89, no. 11, pp. 5815–5875, 2001.

[24] F. Bernardini, V. Fiorentini, and D. Vanderbilt, "Accurate calculation of polarization-related quantities in semiconductors," *Phys. Rev. B*, vol. 63, pp. 193 201–193 201, 2001.

[25] S. Shokhovets, R. Goldhahn, G. Gobsch, S. Piekh, R. Lantier, A. Rizzi, V. Lebedev, and W. Richter, "Determination of the anisotropic dielectric function for wurtzite AlN and GaN by spectroscopic ellipsometry," *J. Appl. Phys.*, vol. 94, no. 1, pp. 307–312, 2003.

[26] A. S. Barker, Jr. and M. Ilegems, "Infrared lattice vibrations and free-electron dispersion in GaN," *Phys. Rev. B*, vol. 7, pp. 743–750, 1973.

[27] S. Strite and H. Morkoç, "GaN, AlN, and InN: A review," *J. Vac. Sci. Technol. B*, vol. 10, pp. 1237–1266, 1992.

[28] T. Takeuchi, H. Takeuchi, S. Sota, H. Sakai, H. Amano, and I. Akasaki, "Optical properties of strained AlGaN and GaInN on GaN," *Jpn. J. Appl. Phys.*, vol. 36, no. 2B, pt. 2, pp. L177–L179, 1997.

[29] D. Korakakis, Jr., K. F. Ludwig, and T. D. Moustakas, "X-ray characterization of GaN–AlGaN multiple quantum wells for ultraviolet laser diodes," *Appl. Phys. Lett.*, vol. 72, no. 9, pp. 1004–1006, 1998.

[30] S. R. Lee, A. F. Wright, M. H. Crawford, G. A. Petersen, J. Han, and R. M. Biefeld, "The band-gap bowing of $Al_xGa_{1-x}N$ alloys," *Appl. Phys. Lett.*, vol. 74, no. 22, pp. 3344–3346, 1999.

[31] G. Bastard, *Wave Mechanics Applied to Semiconductor Heterostructures*. Les Ulis, France: Les Editions de Physique, 1990.

[32] C. Sirtori, F. Capasso, J. Faist, and S. Scandolo, "Non-parabolicity and a sum rule associated with bound-to-bound and bound-to-continuum intersubband transitions in quantum wells," *Phys. Rev. B*, vol. 50, pp. 8663–8674, 1994.

[33] B. Jensen, "The quantum extension of the Drude-Zener theory in polar semiconductors," in *Handbook of Optical Constants of Solids*, E. D. Palik, Ed. San Diego, CA: Academic, 1985, pp. 169–188.

[34] G. Bentoumi, A. Deneuville, B. Beaumont, and P. Gibart, "Influence of Si doping level on the Raman and IR reflectivity spectra and optical absorption spectrum of GaN," *Mater. Sci. Eng.*, vol. B50, no. 1-3, pp. 142–147, 1997.

[35] S. J. Allen, Jr., D. C. Tsui, and B. Vinter, "On the absorption of infrared radiation by electrons in semiconductor inversion layers," *Solid State Commun.*, vol. 20, pp. 425–428, 1976.

[36] T. Ido, S. Tanaka, M. Suzuki, M. Koizumi, H. Sano, and H. Inoue, "Ultra-high-speed multiple-quantum-well electro-absorption modulators with integrated waveguides," *J. Lightw. Technol.*, vol. 14, no. 9, pp. 2026–2034, Sep. 1996.

[37] F. Dorgeuille and F. Devaux, "On the transmission performances and the chirp parameter of a multiple-quantum-well electroabsorption modulator," *IEEE J. Quantum Electron.*, vol. 30, no. 11, pp. 2565–2572, Nov. 1994.

[38] F. Koyama and K. Iga, "Frequency chirping in external modulators," *J. Lightw. Technol.*, vol. 6, no. 1, pp. 87–93, Jan. 1988.

[39] J. Kim, M. Lerttamrab, S. L. Chuang, C. Gmachl, D. L. Sivco, F. Capasso, and A. Y. Cho, "Theoretical and experimental study of optical gain and linewidth enhancement factor of type-I quantum-cascade lasers," *IEEE J. Quantum Electron.*, vol. 40, no. 12, pp. 1663–1674, Dec. 2004.

[40] Y. Miyazaki, H. Tada, S. Tokizaki, K. Takagi, T. Aoyagi, and Y. Mitsui, "Small-chirp 40-Gbps electroabsorption modulator with novel tensile-strained asymmetric quantum-well absorption layer," *IEEE J. Quantum Electron.*, vol. 39, no. 6, pp. 813–819, Jun. 2003.

[41] J. Hamazaki, S. Matsui, H. Kunugita, K. Ema, H. Kanazawa, T. Tachibana, A. Kikuchi, and K. Katsumi, "Ultrafast intersubband relaxation and nonlinear susceptbility at 1.55 μm in GaN–AlN multiple-quantum wells," *Appl. Phys. Lett.*, vol. 84, no. 7, pp. 1102–1104, 2004.

[42] N. Suzuki, N. Iizuka, and K. Kaneko, "FDTD simulation of femtosecond optical gating in nonlinear optical waveguide utilizing intersubband transition in AlGaN–GaN quantum wells," *IEICE Trans. Electron.*, vol. E83-C, no. 6, pp. 981–988, 2000.

[43] R. J. Warburton, K. Weilhammer, C. Jabs, J. P. Kotthaus, M. Thomas, and H. Kroemer, "Collective effects in intersubband transitions," *Physica E*, vol. 7, no. 1–2, pp. 191–199, 2000.

Petter Holmström received the M.Sc. degree in engineering physics and the Ph.D. degree in electrical engineering from the Royal Institute of Technology (KTH), Stockholm, Sweden, in 1996 and 2003, respectively. The subject of his Ph.D. thesis was "high-speed modulators based on intersubband transitions."

He is currently a Postdoctoral Fellow at the Department of Electrical and Electronics Engineering, Sophia University, Tokyo, Japan. His research interests include intersubband transitions and their applications for optical communication, as well as plasmonics to achieve strongly confining optical waveguides.